Strain Distribution within Geosynthetic-Reinforced Slopes

Jorge G. Zornberg, M.ASCE,[1] and Fabiana Arriaga[2]

Abstract: Geosynthetic-reinforced slopes are conventionally designed using methods based on limit equilibrium. In order to estimate the factor of safety against internal stability using these methods, the distribution of the reinforcement peak tensile forces with height must be assumed. A linear distribution of reinforcement peak tension with height, with zero tension at the crest and maximum peak tension at the toe of the structure, has often been assumed. Although this assumption may be appropriate for the design of vertical geosynthetic-reinforced walls, little evidence has been collected so far justifying this distribution for the design of geosynthetic-reinforced slopes. A combination of centrifuge testing and digital image analysis is undertaken in order to obtain the strain distribution within geosynthetic-reinforced slopes under prefailure conditions. Specifically, digital image analysis techniques are used to determine the displacement distribution along reinforcement layers in reduced-scale models subjected to increasing *g* levels. A sigmoid function was useful to fit raw displacement data and estimate the strain distribution along reinforcement layers. Analysis of reinforcement strain results shows that the location of the reinforcement maximum peak strain does not occur near the toe of the structure, but was located approximately at midheight of the reinforced slopes, at the point along the critical failure surface directly below the crest of the slope. The pattern of reinforcement peak strain with height obtained for prefailure conditions is similar to that obtained for failure conditions. The estimated factor of safety is found to be a good indicator of the magnitude of the reinforcement maximum peak strain for geosynthetic-reinforced slopes built with different configurations.

DOI: 10.1061/(ASCE)1090-0241(2003)129:1(32)

CE Database keywords: Geosynthetics; Slopes; Strain distribution.

Introduction

The acceptance of geosynthetics in reinforced soil construction has been triggered by a number of factors, including aesthetics, reliability, cost, simple construction techniques, good seismic performance, and the ability to tolerate large deformations without structural distress. Field monitoring studies of reinforced soil structures, however, have posed major challenges, particularly regarding the monitoring of tensile stresses and strains of the geosynthetics.

Intrusive field instrumentation techniques have been used for the monitoring of strains within full-scale geosynthetic-reinforced soil structures. However, the costs associated with full-scale instrumentation may be significant and the reliability of the collected data has often been questionable. As a result, comparatively few prototype structures have been monitored and the current understanding of the strain distribution within reinforcement layers under working stress conditions is possibly inaccurate and largely ''presumed.'' Among the different types of reinforced soil systems, the lack of field data is particularly striking for the case of geosynthetic-reinforced soil slopes, which may result in significant inaccuracies in their design. Comparatively high reduction factors and factors of safety have been incorporated into current design methodologies. Use of these factors has rendered safe, though overconservatively designed reinforced soil structures.

Centrifuge modeling in combination with digital image analysis is used in this investigation as an alternative to field instrumentation in order to obtain the distribution of strains within geosynthetic-reinforced soil slopes under prefailure conditions. The centrifuge provides a controlled environment in which structures can be studied as scaled-down models while preserving prototype stress levels. Specifically, this study involves the analysis of digital video documentation of displacement fields collected during centrifuge testing of reduced-scale geosynthetic-reinforced soil slopes. The focus is on defining the pattern of reinforcement strains under prefailure, working stress conditions. Analysis of the digital images allowed the determination of the following information for increasing g levels (i.e., decreasing factors of safety): (1) strain distribution along each reinforcement layer, which typically shows a well-defined peak strain value; (2) distribution with height of reinforcement peak strains within the geosynthetic-reinforced soil slope, which has often been assumed to have a triangular pattern; and (3) the magnitude and location (i.e., height) of the reinforcement maximum peak strain that develops within the entire structure. The term ''peak strain'' is used herein to denote the maximum strain that develops along each of the several reinforcement layers in the structure. On the other hand, the term ''maximum peak strain'' is used to denote the overall maximum strain that develops among all reinforcement layers.

This paper initially evaluates information gathered from instrumented full-scale geosynthetic-reinforced soil slopes that provide reinforcement strain distribution data. Subsequently, an over-

[1]Assistant Professor, Univ. of Colorado at Boulder, Dept. of Civil, Environmental and Architectural Engineering, Campus Box 428, Boulder, CO 80309. E-mail: jorge.zornberg@colorado.edu

[2]Graduate Student, Univ. of Colorado at Boulder, Dept. of Civil, Environmental and Architectural Engineering, Campus Box 428, Boulder, CO 80309.

Note. Discussion open until June 1, 2003. Separate discussions must be submitted for individual papers. To extend the closing date by one month, a written request must be filed with the ASCE Managing Editor. The manuscript for this paper was submitted for review and possible publication on November 8, 2001; approved on April 20, 2002. This paper is part of the ***Journal of Geotechnical and Geoenvironmental Engineering***, Vol. 129, No. 1, January 1, 2003. ©ASCE, ISSN 1090-0241/2003/1-32–45/$18.00.

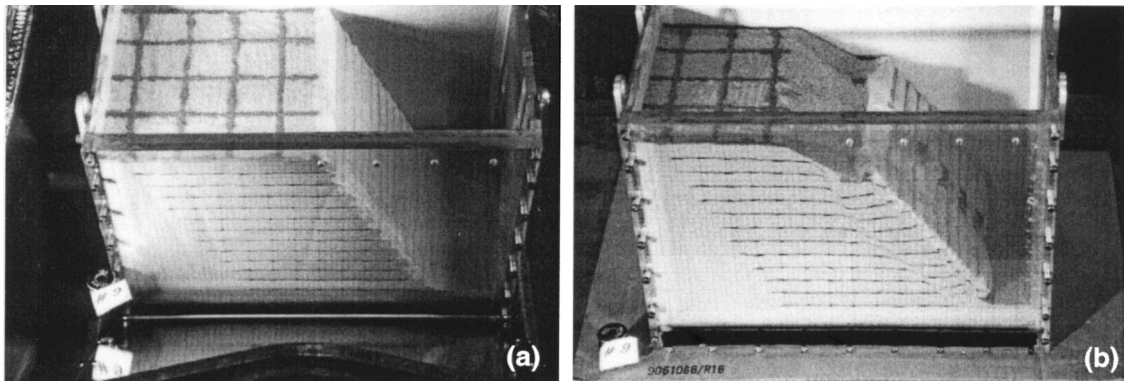

Fig. 1. Reinforced slope model: (a) before testing in a geotechnical centrifuge and (b) after testing, showing development of failure surface

view is presented of the aspects of a centrifuge testing program that are relevant for the analysis of reinforcement strain distributions. Details of the digital image analysis of centrifuge models, including procedures followed to obtain reinforcement displacement and strain distributions, are presented next. Finally, reinforcement strain distribution results obtained for prefailure conditions and their implications in current design methods of geosynthetic-reinforced slopes are evaluated.

Reinforcement Tension Distribution in Reinforced Soil Slope Design

The effect of geosynthetic reinforcements on the stability of a steep slope is illustrated in Fig. 1(a), which shows a reduced-scale geosynthetic-reinforced slope model built using dry sand as backfill material. Horizontal geosynthetic reinforcements placed within the backfill provide stability to the steep slope, the inclination of which is well above the angle of repose of the sand. In fact, the reinforced slope model not only did not fail under its own weight, but its failure only occurred after the unit weight of the backfill was increased 66 times by placing the model in a geotechnical centrifuge (Zornberg et al. 1998a). Fig. 1(b) shows the failure surface developed in the reinforced slope model following centrifuge testing. The observed failure mechanism validated experimentally the mechanism assumed in reinforced soil design, which is typically performed using limit equilibrium.

When the stability of unreinforced soil slopes is analyzed by limit equilibrium methods, assumptions concerning the shape of the failure surface and the inclination and magnitude of the interslice forces are required in order to obtain a solution. Most reinforced soil stability analyses are modified versions of classical limit equilibrium slope stability methods in which reinforcement tensile forces are introduced in the calculations. The main objective of the design of geosynthetic-reinforced slopes is to define the layout and required tensile strength of the reinforcements. The stability analysis of reinforced slopes needs additional assumptions on top of those already made for the analysis of unreinforced slopes. These additional assumptions include the inclination (e.g., horizontal, tangential) and the distribution with height (e.g., linear, uniform) of the reinforcement peak tensile force along the potential failure surface (Christopher and Leshchinsky 1991). Parametric limit equilibrium analyses (Wright and Duncan 1991) and evaluation of centrifuge test results (Zornberg et al. 1998b) have shown that the assumed orientation of the tensile forces does not affect significantly the calculated factor of safety, at least for structures with granular backfills. However, the assumed distribution with height of reinforcement peak tensile forces may have important implications in design, particularly when zones of different reinforcement density within the height of the reinforced soil structure are used.

Current design methods for reinforced soil vertical walls are based on the assumption that reinforcement peak forces are proportional to the overburden pressure, as measured from the top of the vertical wall [Fig. 2(a)]. The rationale behind this assumption is that extensible reinforcements should resist the active earth pressure in the soil (e.g., Collin 1997; Elias et al. 2001). Although interaction with the foundation soils has been found to affect this distribution in the lower reinforcement layers, studies have indicated that maximum tensile forces are well predicted by assuming a Rankine active condition in geosynthetic-reinforced vertical walls (e.g., Allen et al. 1991; Zornberg and Mitchell 1994).

In the case of reinforced soil slopes, which have their design based on limit equilibrium and not on working stress methodologies, a reinforcement peak tension distribution with height must also be assumed. Extending the rationale used for the design of reinforced soil vertical walls, the triangular distribution shown in Fig. 2(a) has also been typically assumed for the design of reinforced soil slopes. This distribution has been assumed, for example, in design charts for geosynthetic-reinforced soil slopes developed using limit equilibrium approaches (Schmertmann et al. 1987; Leshchinsky and Boedeker 1989; Jewell 1991). A similar distribution was also adopted by FHWA design guidelines for reinforced soil slopes higher than 6 m (Elias et al. 2001).

However, the conventional triangular distribution of reinforcement peak forces with height is not supported by a centrifuge investigation that evaluated the behavior of reinforced soil slopes at failure (Zornberg et al. 1998a). In that study, failure was observed to initiate from midheight of the slopes, which led to proposing the distribution of reinforcement forces with height shown in Fig. 2(b). This distribution was inferred from the analysis of slope models [Fig. 2(c)], which had been brought to a failure condition [i.e., factor of safety (FS) = 1.0]. However, no quantitative information has been collected so far on the distribution of tensile forces or strains for geosynthetic-reinforced slopes under working stress conditions (e.g., FS = 1.5 or higher).

In summary, performance data of geosynthetic-reinforced slopes under prefailure conditions is needed to assess the strain distribution along reinforcement layers, the distribution of reinforcement peak strain with height within the entire structure, and the magnitude and location of the maximum peak strain developed among all reinforcement layers. Probably the best way to investigate the strain distribution within geosynthetic-reinforced

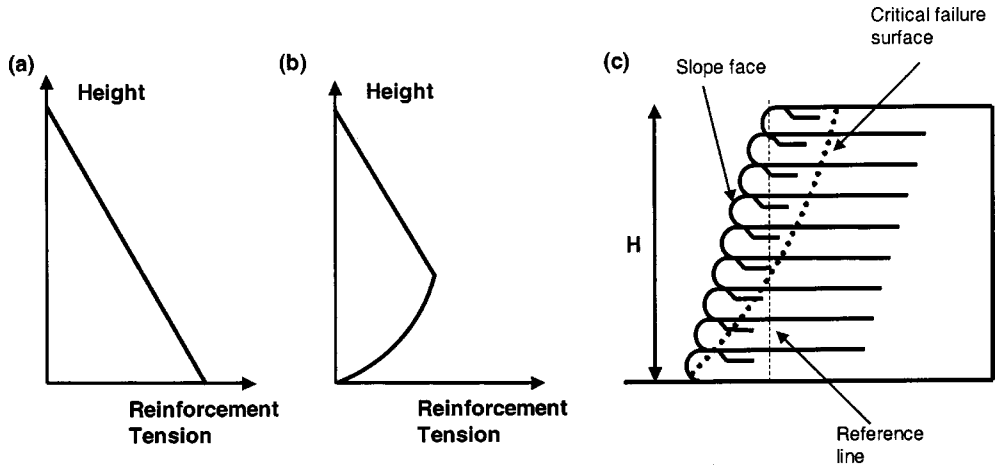

Fig. 2. Distribution of reinforcement peak tension with height: (a) for geosynthetic-reinforced walls (used in design); (b) for geosynthetic-reinforced slopes (proposed); and (c) schematic cross section

soil slopes is by monitoring of full-scale prototypes. Accordingly, an assessment is conducted as part of this study of full-scale structures for which geosynthetic strain monitoring has been reported. In addition, and considering the limited amount of data available from instrumented full-scale projects, information on reinforcement strain distribution is generated and evaluated from reduced-scale geosynthetic-reinforced models tested in a geotechnical centrifuge.

Assessment of Reinforcement Strains From Monitored Full-Scale Geosynthetic-Reinforced Slopes

Although field instrumentation projects have provided significant information regarding the reinforcement strain distribution within geosynthetic-reinforced vertical walls (e.g., Allen et al. 1991; Bathurst et al. 1992; Fishman et al. 1993; Zornberg and Mitchell 1994), comparatively scarce monitoring data has been collected on the strain distribution within geosynthetic-reinforced soil slopes. Instrumentation data from full-scale geosynthetic-reinforced soil slopes reported in the technical literature are compiled in Table 1. Only studies that included monitoring of the strain distribution within the reinforcement layers and that allowed determination of the magnitude and location of the reinforcement maximum peak strain are summarized in the table. The table summarizes the type of backfill, geosynthetic reinforcement, and facing of the monitored structures. In the case of composite structures, the toe of the overall system was considered for the purpose of defining the total slope height.

Assessment of strain distribution results indicates, as expected, that the strain magnitude along reinforcement layers increases with increasing loading (Fannin and Hermann 1990; Zornberg and Kavazanjian 2001). Also, the strain distribution along reinforcement layers usually exhibits a well-identified peak value (Miki et al. 1988; Fannin and Hermann 1990; Zornberg et al. 1995; Ghinelli and Sacchetti 1998). The distribution of reinforcement strains in geosynthetic-reinforced slopes with rigid facing shows a comparatively high strain at the connection of reinforcement layers with rigid facing units (Fannin and Hermann 1990). High connection strains have been attributed to the relative down-

Table 1. Full-Scale Geosynthetic-Reinforced Slopes with Reported Reinforcement Strain Distribution Information

	Slope height, H (m)	Slope angle (H:V)	Reinforcement type	n	Backfill material	Facing	ε_{max} (%)	Location of ε_{max} (% of H)	Reference
1	2.7	0.84:1	W	6	Gravel	Flexible	0.60	57	Delmas et al. 1988
2	6.0	0.5:1	GG	4	Sand	Flexible	0.90	17	Fannin and Hermann 1988
3	3.0	0.7:1	GG	2	Sand	Flexible	0.30	67	Miki et al. 1988
4	3.0	0.7:1	GG	3	Sand	Flexible	0.20	50	Miki et al. 1988
5	4.8	0.5:1	GG	5	Sand	Flexible	0.40	50	Fannin and Hermann 1990
6	4.8	0.5:1	GG	8	Sand	Flexible	0.65	38	Fannin and Hermann 1990
7	7.6	0.5:1	GG	9	Silt	Flexible	0.69	40	Christopher et al. 1994
8	7.6	0.5:1	W	9	Silt	Flexible	0.69	40	Christopher et al. 1994
9	6.8	0.5:1	GG	10	Fine grained	Rigid	0.35	35	Kasahara et al. 1994
10	27.4	1:1	NW	50	Decomposed granite	Flexible	0.20	60	Barrows and Lofgren 1993; Zornberg et al. 1995
11	5.3	0.58:1	GG	8	Fine grained	Flexible	1.60	25	Ghinelli and Sacchetti 1998
12	5.6	0.58:1	GG	8	Fine grained	Flexible	1.00	46	Ghinelli and Sacchetti 1998
13	4.6	0.75:1	GG	11	Gravel	Flexible	0.40	59	Zornberg and Kavazanjian 2001

Note: n=number of reinforcement layers; ε_{max}=maximum peak strain; W=woven geotextile; NW=nonwoven geotextile; GG=geogrid; H:V=horizontal to vertical.

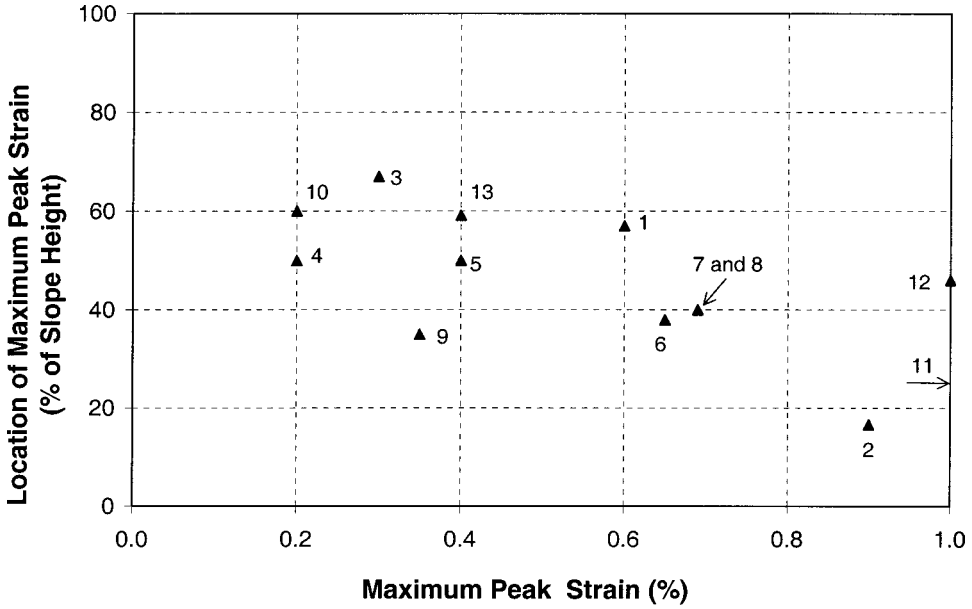

Fig. 3. Magnitude and location of reinforcement maximum peak strain for full-scale geosynthetic-reinforced slopes under working stress conditions. (Note: Full-scale structures are those listed in Table 1).

ward movement of the retained soil with respect to the less compliant panel structures (Bathurst 1992). For geosynthetic-reinforced slopes with flexible facing systems, the location of the reinforcement peak strain moves away from the slope face. The locus of reinforcement peak strains generally coincides with the location of the potential failure surface.

Of particular relevance for the purpose of this investigation is to evaluate the magnitude and location of the reinforcement maximum peak strains. Fig. 3 shows that the magnitude of the reinforcement maximum peak strain for structures listed in Table 1. The maximum peak strain, generally monitored under working stress conditions, is typically below 1%. This strain value is well below the strain level that corresponds to the maximum tensile strength of typical geosynthetic materials. Fig. 3 also shows the location, measured vertically from the toe as a percentage of the structure height, of the reinforcement layer that achieves the maximum peak strain. The location of the maximum peak strain ranges from approximately 20 to 60% of the structure height. This indicates that the common assumption that the reinforcement maximum peak tensile force occurs at the toe of geosynthetic-reinforced slopes is not valid for working stress conditions. Even though the number of data points is limited, it appears that there is no significant correlation between the magnitude and location of the reinforcement maximum peak strain.

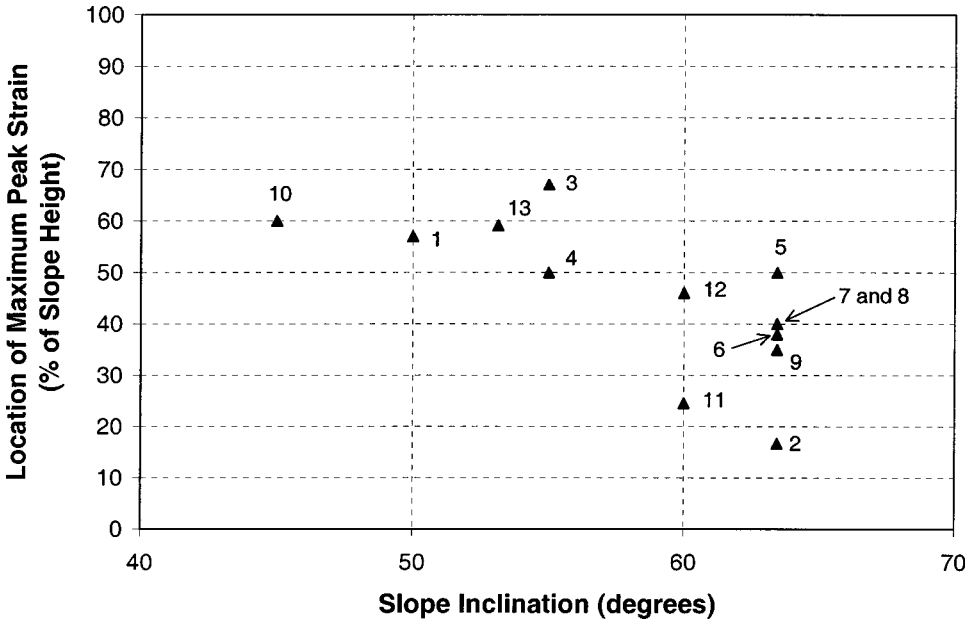

Fig. 4. Location of maximum peak reinforcement strain as function of inclination of slope face for full-scale geosynthetic-reinforced slopes. (Note: Full-scale structures are those listed in Table 1).

Fig. 4 shows the location, as a percentage of the structure height, of the reinforcement maximum peak strain as a function of the slope inclination for structures listed in Table 1. The trend observed from this data, collected from full-scale structures under working stress conditions, suggests that the location of the reinforcement maximum peak strains is a function of the slope inclination. Such a trend is consistent with the distribution shown in Fig. 2(b), inferred from the results of reduced-scale centrifuge models under failure condition.

In summary, available data on reinforcement strain distribution within geosynthetic-reinforced slopes does not support the current design assumption that the reinforcement maximum peak tension is located at the toe of the structures. Instead, such location appears to be a function of the inclination of the slope. However, definite conclusions cannot be drawn from available field information because of the limited number and different characteristics of available instrumented structures. Consequently, additional information on the strain distribution within geosynthetic-reinforced slopes under working stress conditions is generated in this study from reduced-scale geosynthetic-reinforced slope models tested in a geotechnical centrifuge.

Table 2. Characteristics of Centrifuge Geotextile-Reinforced Slope Models

	Model B18	Model B12	Model D12	Model S9
Number of reinforcement layers	18	12	12	9
Vertical spacing (mm)	12.70	19.05	19.05	25.40
Reinforcement type	weak	weak	weak	strong
Reinforcement tensile strength (kN/m)	0.123	0.123	0.123	0.183
Relative density of sand (%)	55	55	75	55
Sand peak friction angle	35°	35°	37.5°	35°
g level at failure (N_f)	76.5	60	66	52.5
Elapsed time until failure (min)	53	43	60	39
Failure type	catastrophic	catastrophic	catastrophic	progressive

Centrifuge Modeling of Geosynthetic-Reinforced Soil Slopes

Small-scale physical modeling of engineered earth structures has been used in the past to provide insight into the behavior of reinforced soil structures (e.g., Lee et al. 1973; Juran and Christopher 1989). However, a limitation of scaled physical models under 1-g conditions is that stress levels in the models are much smaller than in full-scale structures, thus leading to different soil properties and loading conditions. The centrifuge provides a tool for geotechnical modeling in which prototype structures can be studied as scaled-down models while preserving prototype stress levels. Although modeling limitations are often difficult to overcome when the purpose of the investigation is to compare the performance of model and prototype structures, many of these limitations can be taken into account when the purpose is to validate analytical tools and the qualitative behavior of geotechnical systems (Zornberg et al. 1997).

A wide range of geotechnical problems has been investigated using centrifuge modeling techniques, and evaluation of the behavior of reinforced soil structures is no exception. Several of the previous centrifuge studies have focused on the validation of design methods (e.g., Bolton et al. 1978; Mitchell et al. 1988; Zornberg et al. 1998b), other studies have evaluated the effect of specific design parameters (e.g., Goodings and Santamarina 1989; Güler and Goodings 1992; Porbaha and Goodings 1996), while others have investigated the performance of structures subjected to loadings other than self weight such as concentrated or seismic loads (e.g., Kutter et al. 1990; Ragheb and Elgamal 1991; Law et al. 1992; Nova-Roessig and Sitar 1998). However, a comprehensive review of previous centrifuge studies on the performance of reinforced soil structures (Zornberg et al. 1997) indicates that no previous research has been conducted on the evaluation of strain distribution within reinforced soil slopes under working stress conditions.

While this investigation focuses on the evaluation of the performance of geosynthetic-reinforced slope models under prefailure conditions, it builds upon previous studies on the evaluation of those models under failure conditions (Zornberg et al. 1998b). The centrifuge study under failure conditions provided strong evidence that limit equilibrium methodologies adequately predict the collapse of geosynthetic-reinforced soil structures. The study presented herein extends the previous investigation by evaluating the performance of geosynthetic-reinforced slopes under working stress conditions and, specifically, the strain distribution of geosynthetic reinforcements under prefailure conditions.

The geosynthetic-reinforced slope models analyzed in this investigation were built with the same geometry and were subjected to a gradually increasing centrifugal acceleration until failure occurred. A box with inside dimensions of 419 mm$\times$203 mm in plan, and 300 mm in height was used to contain the models. A transparent Plexiglas plate was used as one of the side walls of the box to enable in-flight visualization of the models during testing. The remaining walls of the box were aluminum plates lined with polytetrafluorethylene to minimize side friction. The Plexiglas wall was lined with a Mylar sheet overprinted with a square grid pattern, which was used as a reference for monitoring displacements within the backfill. In order to prevent scratches and to minimize side friction, a second Mylar sheet was placed over the one with the square grid pattern. The total height of the models was 254 mm (228.6-mm-high geotextile-reinforced slopes built on a 25.4-mm-thick foundation layer). The slope inclination of the models was 1H:2V (horizontal to vertical). Air dried Monterey No. 30 sand was used as backfill material and foundation soil. The number of reinforcement layers in the models ranged from nine to eighteen, which corresponds to reinforcement spacings ranging from 25.4 to 12.7 mm. All models were built using a reinforcement length of 203 mm. The selection of relatively long reinforcements was intentional, as the testing program aimed at avoiding the development of external or compound failure surfaces (i.e., the slopes were designed to fail by reinforcement breakage). The geotextile layers were wrapped at the face using 50-mm-long overlaps. The characteristics of the models evaluated using digital image analysis are summarized in Table 2. The model designation uses a letter that identifies whether the model belongs to the baseline series (B), to the denser backfill series (D), or to the stronger geotextile series (S). The number that follows in the model designation refers to the number of reinforcement layers.

Due to the small size of the model slopes, internal instrumentation could not be included to monitor the performance of the

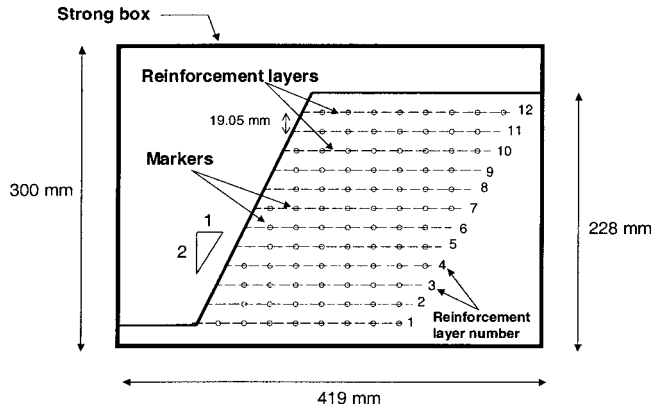

Fig. 5. Geometry of centrifuge slope Model B12

models under working stress levels. It was, for example, impossible to instrument the reinforcement layers due to their small width and high fragility. The difficulty in instrumenting geosynthetic reinforcements in centrifuge models has also been reported by other investigators (e.g., Mahmud and Zimmie 1998). Instead, an image acquisition system was used to track movements of colored sand markers through the Plexiglas wall. Green-colored sand was placed against the Plexiglas wall along each reinforcement layer. In addition, black-colored sand markers were placed at a regular horizontal spacing of 25 mm and were carefully matched during construction with the corners of the square grid. The geometric configuration of one of the models (Model B12) is shown in Fig. 5.

The models were subjected to gradually increasing centrifugal acceleration levels. After reaching each level, the models were held at a constant acceleration for approximately two minutes to allow equalization of the load. As the models deformed, the black sand markers moved with the adjacent soil. Testing progressed until failure of the models occurred. Careful postfailure assessment of the models indicated that efforts to minimize side friction were successful (Zornberg et al. 1998a). In fact, tears in the geotextile reinforcements were always perpendicular to the direction of loading, showing no evidence of edge effects caused by lateral friction against the walls of the centrifuge box. Also, model dissection revealed that displacements of markers placed within the model were essentially identical to displacements of markers placed against the Plexiglas wall.

An extensive testing program was performed to evaluate the strength properties of the sand backfill material, of the geotextile reinforcements, and of several interfaces that could influence the performance of the slope models (Zornberg et al. 1998b). The centrifuge models were built using Monterey No. 30 sand, which is a clean, uniformly graded sand classified as SP in the Unified System. Monterey No. 30 sand has a uniform gradation curve. The friction angles obtained from triaxial compression tests are 35 and 37.5° for relative densities of 55 and 75%, respectively. Unit weight values for Monterey No. 30 sand at these relative densities are 15.64 and 16.21 kN/m^3, respectively. Commercially available interfacing fabric has been successfully used to simulate reinforcement in centrifuge testing of geosynthetic-reinforced slopes (Güler and Goodings 1992). Two types of nonwoven interfacing fabrics, having a mass per unit area of 24.5 and 28 g/m^2, were selected as reinforcement. Unconfined ultimate tensile strength values, measured from wide-width strip tensile tests ASTM D4595, were 0.063 and 0.119 kN/m for weaker and stronger geotextile, respectively. Confined tensile strength values, obtained from back calculation of failure in the centrifuge slope models, were 0.123 and 0.183 kN/m for the weaker and stronger geotextiles, respectively (Zornberg et al. 1998b). Confined tensile strength values were used for estimating the factor of safety of the models analyzed in this study under increasing g levels.

Digital Image Analysis of Geosynthetic-Reinforced Slope Models

Although digital image analysis techniques have found widespread application in disciplines such as medicine, biology, and geography, applications within civil engineering are more incipient (Mora et al. 1998). However, promising advances involving image-processing techniques have been made in granular soil characterization, including evaluation of porosity, fabric, structure, and uniformity of cohesionless soils (Kemeny et al. 1993; Thomas et al. 1994; Kuo and Frost 1996; Obaidat et al. 1998; Jang et al. 1999). Advances have also been made in the use of digital image analysis for assessment of deformation of granular soils and shear band development (Gustafsson and Knutsson 1994; Raschke et al. 1996; Liang et al. 1997) and for measurement of geomembrane surface roughness (Dove and Frost 1999).

In this investigation, consecutive in-flight images of centrifuge models were used to monitor movements as the g level was increased. This combination of centrifuge testing and digital image processing and analysis is suitable for retrieving information on prefailure reinforcement strain distributions without the need of internal instrumentation. The images were collected from continuous videotaped recording of the centrifuge tests. The specific tasks undertaken as part of this investigation regarding digital image processing and analysis included:

- Capturing images recorded from models videotaped during centrifuge testing.
- Tracking the location and analyzing the displacement of markers at each reinforcement level under increasing g levels. This resulted in a database that includes the location of approximately 50 markers from each captured image, under acceleration fields ranging from 1g to more than 70g.
- Calculating the relative displacements and strain distributions along the reinforcements at increasing g levels using the marker location database.

A subset of four centrifuge models was selected for the digital image analysis in this investigation. This includes Models B18 and B12 from the baseline series, Model D12 from the denser backfill series, and Model S9 from the stronger geotextile series. Table 3 summarizes information regarding analyzed images of geosynthetic-reinforced slope models. The table summarizes the recording time, g level at the time of recording, and the factor of safety corresponding to the g level under evaluation. The factors of safety reported in the table were obtained from limit equilibrium analyses performed using Spencer's method and assuming circular failure surfaces (Zornberg et al. 1998b). Soil shear strength and reinforcement tensile strength parameters used in the limit equilibrium analyses accounted for the soil plane strain condition and for the geotextile confinement within the soil.

The image acquisition system consisted of a closed circuit television camera and video recording device. The television camera was mounted at the center of the rotating structure of the centrifuge. This system provided continuous monitoring of the models while testing was in progress. A 45° inclined mirror was used to view the model in-flight through the Plexiglas wall. Fig. 6

Table 3. Characteristics of Analyzed Images for Models B18, B12, D12, and S9

Frame number	1	2	3	4	5	6	7
			Model B18				
Recording time (min)	6:00	8:00	18:00	21:00	28:00	35:00	42:00
g level	10	14	30	34	49.5	64	71.5
Factor of safety	2.70	2.50	1.43	1.18	1.08	1.04	1.02
Maximum peak strain (%)		6.70	7.60	10.01	12.80	16.78	20.34
			Model B12				
Recording time (min)	4:25	6:00	11:00	19:50	29:50	39:50	
g level	5	10	20	40	54	58	
Factor of safety	2.60	2.15	1.50	1.15	1.05	1.01	
Maximum peak strain (%)		7.50	8.92	10.10	13.70	18.90	
			Model D12				
Recording time (min)	9:00	14:30	21:00	32:00	41:00	51:00	
g level	9	15	23.5	38	49.3	59.3	
Factor of safety	2.17	1.95	1.48	1.10	1.07	1.02	
Maximum peak strain (%)		5.43	8.00	11.85	17.61	21.31	
			Model S9				
Recording time (min)	7:00	9:00	14:00	17:00	23:00	30:00	34:00
g level	11	14	23	27	35.5	42	46
Factor of safety	2.07	1.90	1.41	1.15	1.07	1.04	1.02
Maximum peak strain (%)		3.74	6.52	9.87	14.99	17.70	21.70

shows the centrifuge arm with the television camera, the slant mirror, and a slope model ready for testing. A capturing board was used to convert the videotaped images of the centrifuge tests from analogue to digital format. The resolution of the digitized images was 2,100×2,800 pixels.

The view window of the closed-circuit television camera used to collect images during centrifuge testing did not cover the entire Plexiglas wall. Consequently, some reinforcement layers could not be included in the analysis. Images were recorded up to Layer 14 in Model B18, Layer 9 in Models B12 and D12, and Layer 7 in Model S9. As the arm of the centrifuge spins with increasing angular velocity, the bucket holding the model (supported by hinged pins) swings upward so that the top surface of the model becomes gradually perpendicular to the plane of rotation. Since the camera was located at the center of the centrifuge axis, images of the centrifuge model through the Plexiglas wall could not be captured until the top surface of the model became approximately perpendicular to the plane of rotation. Consequently, the initially available images of each model do not correspond to the beginning of the centrifuge tests.

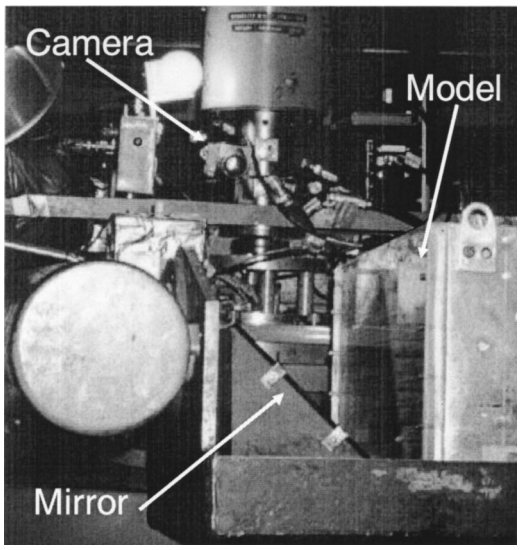

Fig. 6. View of television camera and centrifuge bucket with model and slant mirror in place

In order to define the displacement field within the reinforced soil mass, the edge of the sand markers was identified in subsequent images of the centrifuge models making use of automatic recognition of objects (e.g., edges of sand markers). The center of mass of each sand marker was tracked within the digital images for increasing *g* levels (i.e., decreasing factors of safety). Distance calibration within the images was facilitated by the square grid pattern overprinted on the Mylar sheet used on the Plexiglas wall of the centrifuge models. The analysis of the digital images involved determination of the spatial coordinates of each sand marker for the sequential images captured in the different centrifuge slope models.

Analysis of Results

Reinforcement Displacement Distributions

Relative displacements between sand markers in the geosynthetic-reinforced slopes were defined using the database of marker coordinates obtained for increasing *g* levels. For each reinforcement layer, the marker closest to the face was considered the reference point for determination of relative distances between markers. The distance between the center of mass of each marker and the

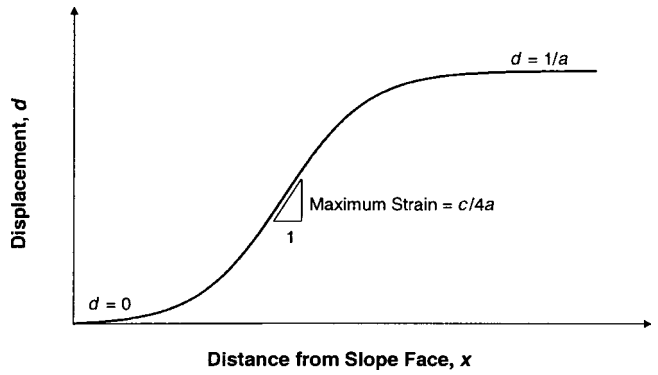

Fig. 7. Features of sigmoid function used to fit displacement data

corresponding reference marker was calculated considering both vertical and horizontal components. The initial coordinates of each marker used for subsequent estimation of reinforcement strains correspond to the initial frame indicated for each model in Table 3. A preliminary evaluation of the reinforcement strains was performed by dividing the relative displacement between consecutive markers by the distance between them. However, minor scatter in the reinforcement displacement distribution resulted in major oscillations in the strain distribution (Zornberg et al. 1995). Consequently, the relative displacement data was fitted to a monotonically increasing function. The expression used to fit the displacement data is a sigmoid function defined by

$$d = \frac{1}{a + be^{-cx}} \tag{1}$$

where d = displacement of each marker relative to the reference marker at the face of the model; x = distance between each marker and the corresponding reference; e = base of natural logarithms; and a, b, and c = fitting parameters. The main characteristics of the sigmoid function are shown in Fig. 7.

Figs. 8(a–d) show displacement results obtained under increasing g levels for four geosynthetic reinforcement layers of Model B12 (Layers 4, 5, 8, and 9). The location of these reinforcement layers is shown in Fig. 5. The solid lines represent raw displacement data, while the dashed lines represent the trend defined by sigmoid functions fitted to the raw data. As anticipated, the measured displacements increase with increasing g levels (i.e., decreasing factors of safety). Displacement data can be fitted reasonably well by sigmoid functions, as shown in the figure for Model B12. Displacement information obtained for all reinforcement layers of the four models evaluated as part of this study is provided by Arriaga and Zornberg (2000).

Reinforcement Strain Distributions

The reinforcement strain distribution along each reinforcement layer was defined using displacement data collected from images captured in-flight during centrifuge testing. Specifically, the geosynthetic strain distribution was calculated from the derivative of the sigmoid function fitted to displacement data. Consistent with the performance data reported in the literature for monitored full-scale geotextile-reinforced slopes with extensible facing, a sigmoid function results in strain distributions tending to zero towards the face and towards the end of the geosynthetic reinforcements. The peak strain value and its location from the slope face in each reinforcement layer can be determined analytically using the parameters a, b, and c that fit the displacement data. The expressions for maximum strain and its location are

$$\varepsilon_{\max} = \frac{c}{4a} \tag{2}$$

$$x_{\max} = \frac{1}{c}\ln\left(\frac{b}{a}\right) \tag{3}$$

where $\varepsilon_{\max}$ = magnitude of the peak strain in each reinforcement and $x_{\max}$ = location, measured from the slope face, where the peak strain occurs. Figs. 9(a–d) show the strain distribution obtained for reinforcement Layers 4, 5, 8, and 9 of Model B12. Layer 8 shows the maximum peak strain obtained for Model B12. Arriaga and Zornberg (2000) provide the reinforcement strain distributions obtained for all reinforcement layers of the four models analyzed in this study. The strain distributions are shown for increasing g levels during centrifuge testing. As anticipated, geosynthetic strain increases with increasing g levels (i.e., decreasing factor of safety). It should be noted, though, that the distance from the slope face of the peak strain remains approximately the same for increasing g levels. This is consistent with limit equilibrium analyses, which show little change in the critical failure surface location for analyses conducted at increasing g levels.

Of particular relevance in the design of geosynthetic-reinforced slopes is the distribution with the height of the reinforcement peak tensile strains. As previously discussed, current design approaches typically assume a triangular distribution with reinforcement maximum peak tension at the toe of the structure. Figs. 10(a–d) summarize the distribution with height of the reinforcement peak tensile strains obtained for Models B18, B12, D12, and S9. The figures show the distribution of peak strain values for increasing g levels (i.e., decreasing factors of safety). The dashed lines in the figures represent the location of the geosynthetic reinforcement layers. As previously mentioned, the collected digital data does not include information from the top and bottom geosynthetic layers. As expected, the results show that reinforcement peak strain values for each reinforcement layer increase for increasing g levels. The distributions of peak tensile strains have a similar pattern with height for increasing g-level values. Also, the pattern of the distribution of maximum tensile strains with height is similar for the different models, which were built with the same slope inclination but with different reinforcement vertical spacing values, different backfill densities, and different reinforcement materials.

Contradicting current design assumptions, the distribution of tensile strains with height does not show a triangular pattern with a maximum value at the toe. Instead, the results obtained for g levels corresponding to prefailure conditions show that the maximum peak strain for each geosynthetic-reinforced model is located approximately at midheight of the slope. The elevation of the reinforcement layers that showed the maximum peak strain ranged from 56 to 58% of the total height of the geosynthetic-reinforced slope. The maximum peak strain obtained for each reinforcement model at different g levels analyzed as part of this study is indicated in Table 3. The patterns of peak strain distribution with height shown in Figs. 10(a–d) for prefailure conditions is consistent with the pattern shown in Fig. 2(b), which had been inferred from evaluation of the failure mechanism observed in the geosynthetic-reinforced models (Zornberg et al. 1998a). The results presented herein validate the distribution shown in Fig. 2(b) by quantifying the magnitude of geosynthetic peak strains for conditions of imminent failure. In addition, these results also ex-

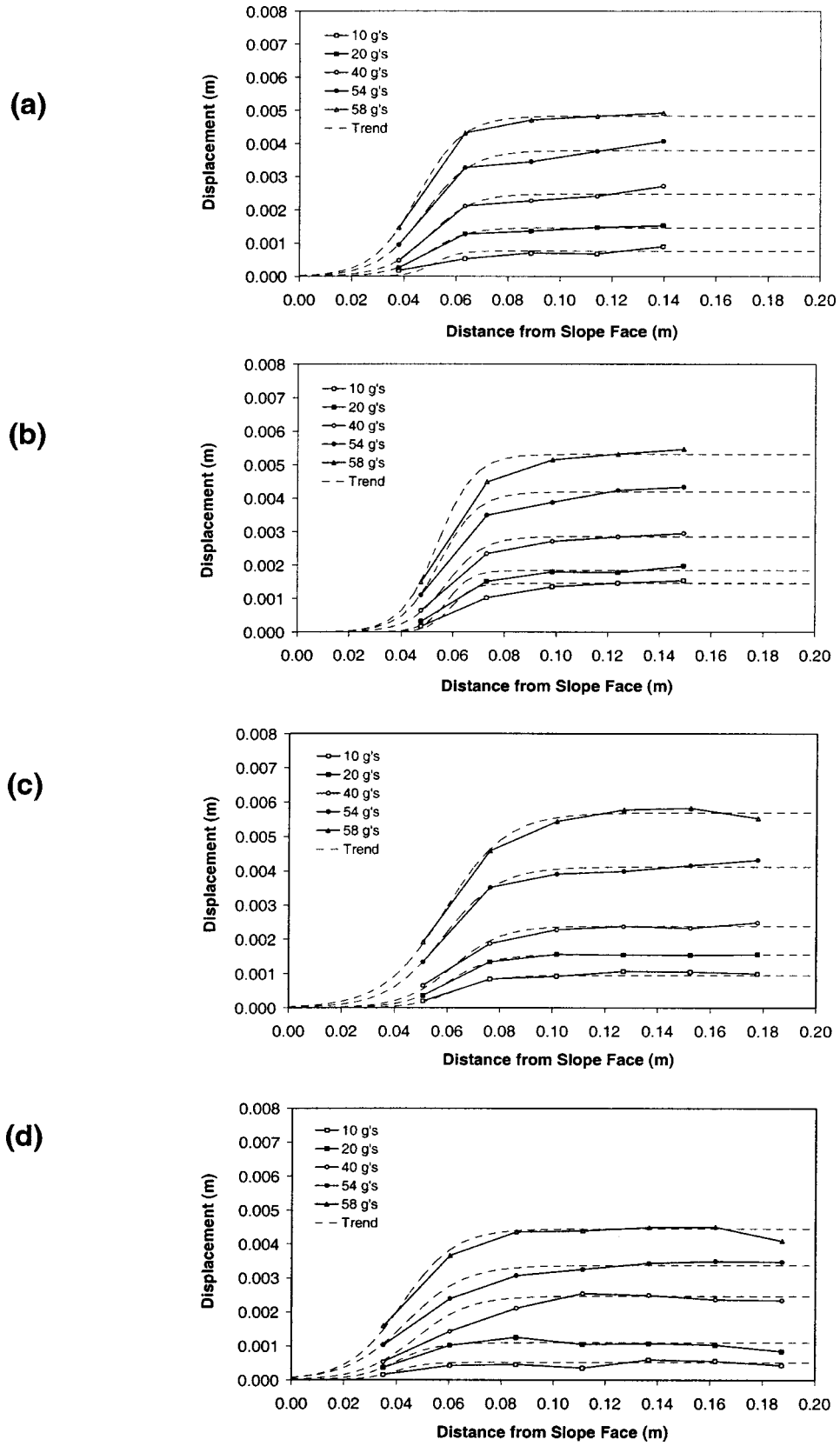

Fig. 8. Displacement data and sigmoid fitted curves for Model B12: (a) reinforcement Layer 9; (b) reinforcement Layer 8; (c) reinforcement Layer 5; and (d) reinforcement Layer 4

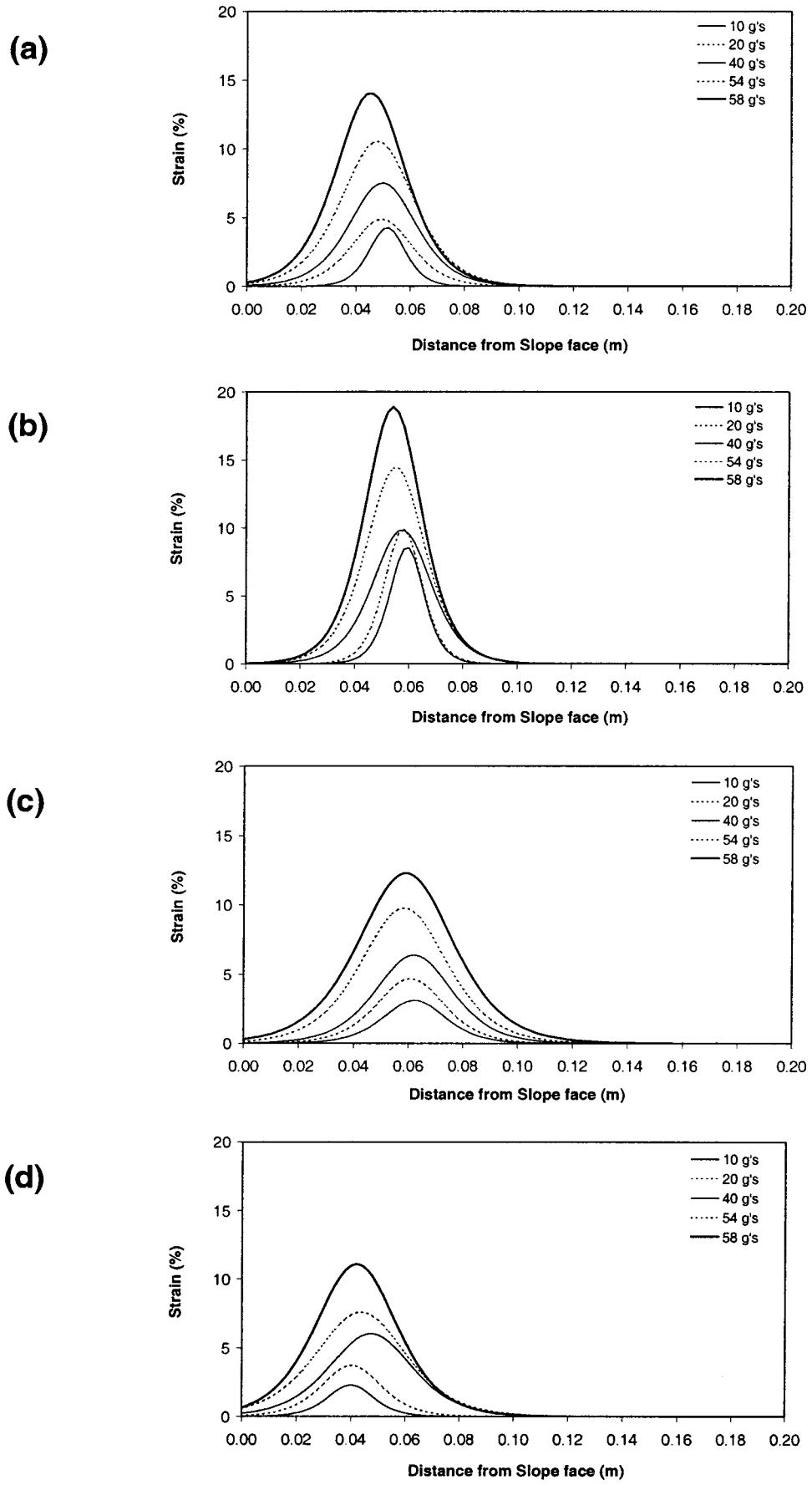

Fig. 9. Strain distribution for Model B12: (a) reinforcement Layer 9; (b) reinforcement Layer 8; (c) reinforcement Layer 5; and (d) reinforcement Layer 4

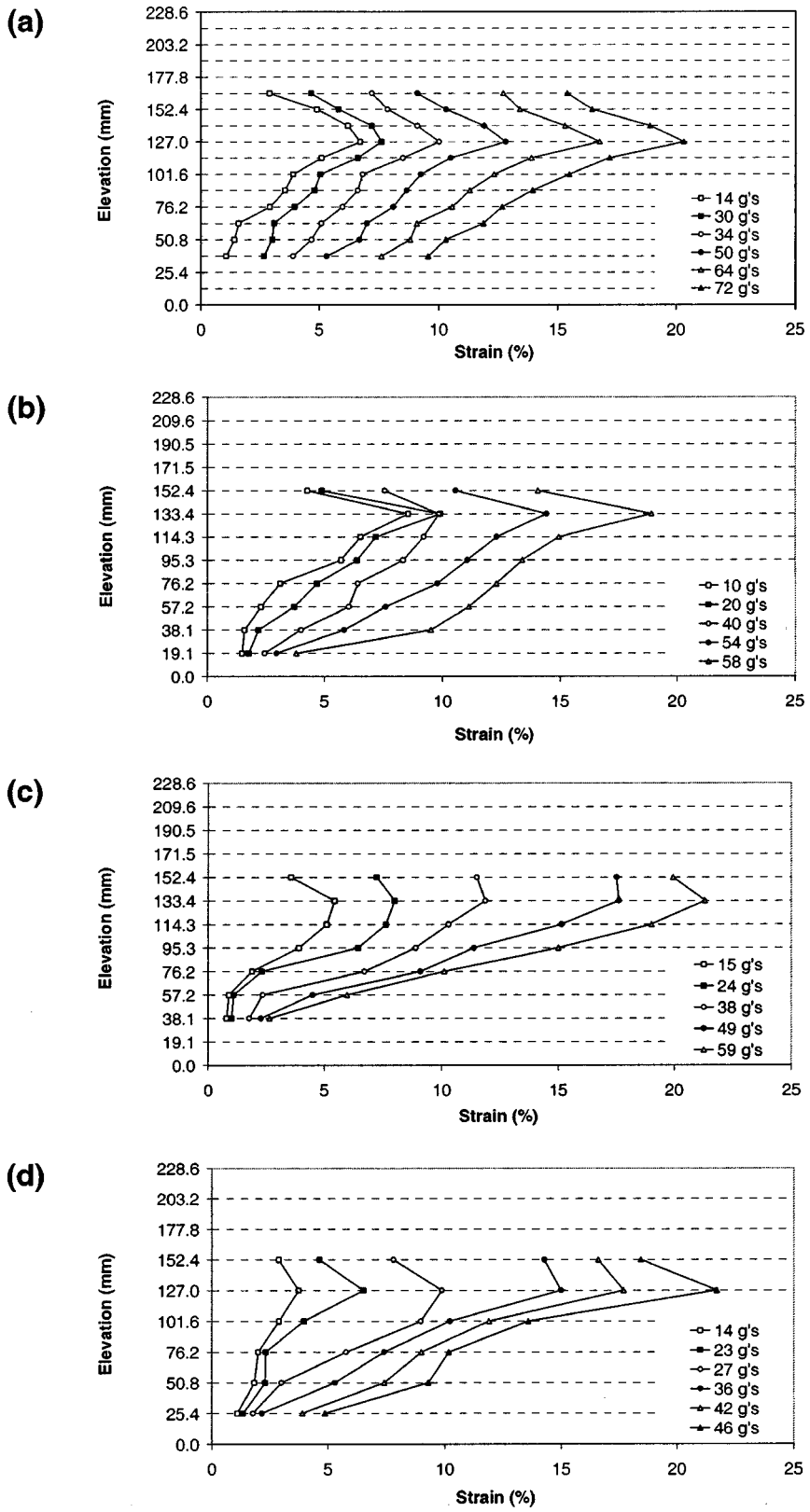

Fig. 10. Reinforcement peak strain distribution: (a) Model B18; (b) Model B12; (c) Model D12; and (d) Model S9

tend the validity of the distribution to prefailure scenarios (i.e., for factors of safety larger than one).

Fig. 11 shows the location of the maximum peak strain for the four centrifuge models analyzed in this study. The locations shown in the figure are for models under *g* levels corresponding to a factor of safety of approximately 1.5. Specifically, the maximum peak strain among all reinforcements is located in reinforcement layer 11 for Model B18, reinforcement Layer 8 for Models B12 and D12, and reinforcement Layer 6 for model S9. The distance from the face to the location of the maximum peak strain varied slightly with increasing *g* levels (i.e., decreasing factors of safety), but the elevation of this location did not change. As

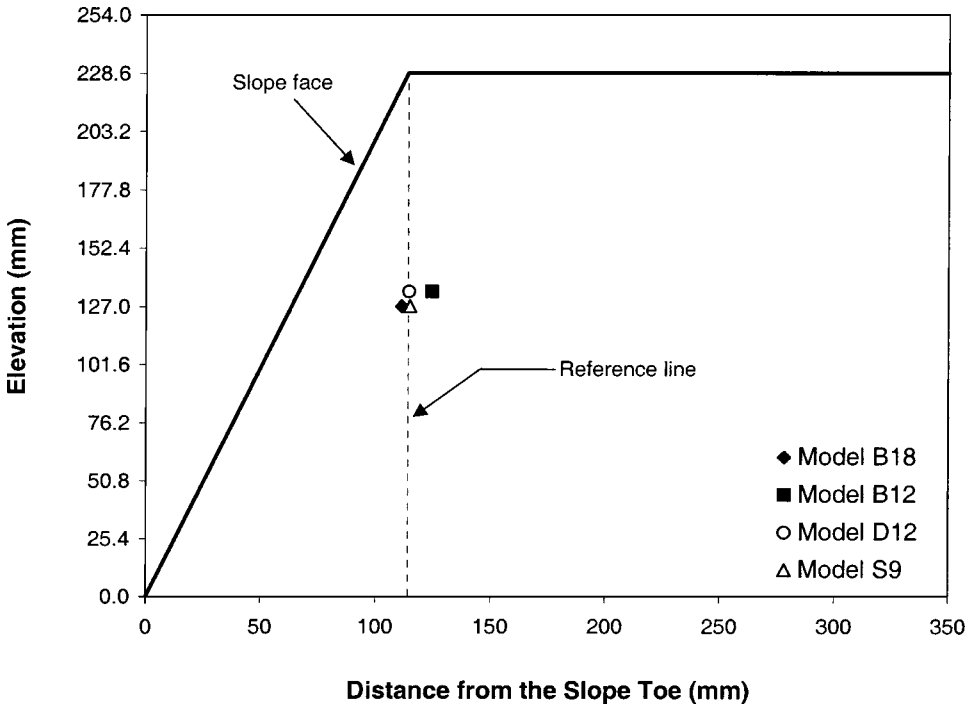

Fig. 11. Location of reinforcement maximum peak strain for Models B18, B12, D12, and S9 (FS approximately 1.5)

shown in the figure, the maximum peak strain occurs approximately below the crest of the slope. This is consistent with the reinforcement tensile force distribution shown in Fig. 2(b), which indicates that the maximum value occurs at a point along the critical failure surface located below the slope crest. An evaluation of local equilibrium between reinforcement forces and horizontal soil stresses also indicates this to be the approximate location of maximum peak strain. In fact, the location of the maximum peak strain (shown in Fig. 11) corresponds approximately to the point along the critical failure surface with the largest overburden pressure. Horizontal soil stresses along the potential failure surface should be proportional to the overburden pressure, which increases approximately with depth below the face of the slope. Accordingly, the maximum peak strain would be located towards the toe of the structure in a vertical reinforced wall, but above the toe of the structure in a reinforced soil slope. In summary, the strain distribution under working stress conditions obtained in this investigation contradicts the triangular distribution with a maximum at the toe of the reinforced slope currently assumed in design [Fig. 2(a)], but provides additional evidence in support of a distribution with a maximum below the crest of the reinforced slope [Fig. 2(b)].

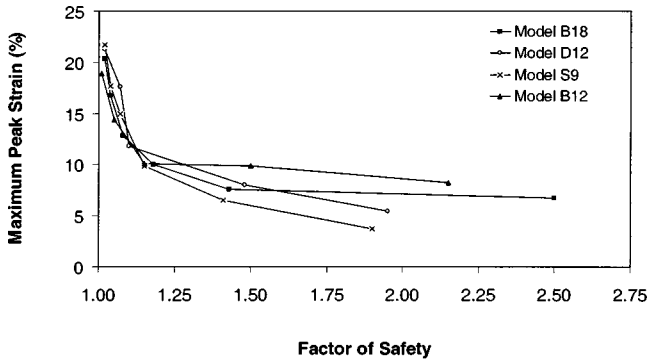

Fig. 12. Reinforcement maximum peak strain with increasing factor of safety for Models B18, B12, D12, and S9

The maximum peak strain values obtained for each geosynthetic-reinforced model are summarized in Fig. 12 as a function of the calculated factor of safety. Despite the different configurations of Models B18, B12, D12, and S9 (reinforcement vertical spacing, reinforcement tensile strength, soil density), the maximum peak strain values appear to show a similar trend for all models. The magnitude of the maximum peak strain that corresponds to a factor of safety of approximately 1.5 is on the order of 8%. This magnitude of geosynthetic strain is higher than typical strain levels reported in the literature for full-scale structures under working stress conditions (on the order of 1%, as shown in Fig. 3). However, this discrepancy can be easily explained because the factors of safety of the centrifuge models in the figure were defined using the ultimate reinforcement tensile strength and the plane strain soil shear strength. Instead, the field performance of full-scale structures under working stress conditions corresponds to the factors of safety defined using design reinforcement and soil strength parameters. This is relevant, particularly considering the major differences between ultimate and design tensile strength parameters in geosynthetic reinforcements. These differences are due to (1) the use of comparatively high reduction factors to define design tensile strength values accounting for creep, durability, and installation damage (combined reduction factors range typically from 5 to 10) and (2) the use of unconfined test results to characterize the reinforcement tensile strength. The tensile strength used for the estimation of the factor of safety in this study did not account for reduction factors and did consider an increased ultimate tensile strength exhibited by nonwoven geotextiles under the confinement of soil (Zornberg et al. 1998b). Although the amount of data presented herein is limited, the consistent trend shown in Fig. 12 suggests that the calculated factor of safety may be a good indicator of the maximum peak strain and,

possibly, of the deformability of geosynthetic-reinforced soil slopes.

Conclusions

Centrifuge testing and digital image analysis were undertaken in order to assess the strain distribution within geosynthetic-reinforced slopes under prefailure conditions. Although data from instrumented full-scale structures is scarce, available information does not support current design assumptions regarding the distribution of reinforcement peak tension with height. This investigation focused on determining this distribution using reduced-scale models subjected to increasing g levels (i.e., decreasing factors of safety). Because of major difficulties associated with the use of intrusive instrumentation to monitor strains within geosynthetic reinforcements, digital image analysis techniques were implemented in this study. The following conclusions can be drawn from the analysis of the data collected as part of this investigation:

- Analysis of available strain monitoring results from full-scale geosynthetic-reinforced soil slopes suggests that the location of the reinforcement maximum peak strain does not occur near the toe of the structure, as assumed by current design methods.
- Analysis of strain results collected using digital image analysis from reduced-scale geosynthetic-reinforced soil slope models also indicates that the location of the reinforcement maximum peak strain does not occur near the toe of the structure.
- The reinforcement peak strain in geosynthetic-reinforced slope models tested in this investigation was consistent with the overburden pressures along potential failure surfaces. Accordingly, the reinforcement maximum peak strain was located approximately at the point along the potential failure surface below the crest of the slope, i.e., where overburden pressures are highest.
- Sigmoid functions were useful to estimate the reinforcement strain distribution as the derivative of the smoothed displacement function.
- The pattern of reinforcement peak strain with height obtained for prefailure conditions was similar to that obtained for failure conditions.
- Similar magnitude and location of the reinforcement maximum peak strain was obtained for the different geosynthetic-reinforced models, even though the models had different reinforcement layout, different backfill soil densities, and different reinforcement tensile strength.
- The estimated factor of safety was a good indicator of the maximum peak strain values in the reinforcements for geosynthetic-reinforced slopes built with different configurations.

Acknowledgments

Support for this research was provided by the National Science Foundation under Grant No. CMS-0070248, the Colorado Advanced Software Institute (CASI), and Bowman Construction, Inc. This financial support is gratefully acknowledged. Technical insight provided by Dean Sandri is also greatly appreciated.

References

Allen, T. M., Christopher, B. R., and Holtz, R. D. (1991). ''Performance of a 12.6 m high geotextile wall in Seattle, Washington.'' *Int. Symposium on Geosynthetic-Reinforced Soil Retaining Walls*, A.A. Balkema, Rotterdam, The Netherlands, 81–100.

Arriaga, F., and Zornberg, J. G. (2000). ''Reinforced soil design: Integration of digital image analysis, numerical modeling, and limit equilibrium.'' *Geotechnological Research Rep.*, Dept. of Civil, Environmental and Architectural Engineering, Univ. of Colorado at Boulder, Colo.

Barrows, R. J., and Lofgren, D. C. (1993). ''Salmon-Lost Trail Pass Highway Idaho Forest Highway 30 Earth Retention Structures Report.'' *Geotechnological Rep. No. 20-92*, FHWA, U.S. Dept. of Transportation, Washington, DC.

Bathrust, R. J. (1992). ''Case study of a monitored propped panel wall.'' *Proc., Int. Symposium on Geosynthetic-Reinforced Soil Retaining Walls*, J. T. H. Wu, ed., Denver, 159–166.

Bathrust, R. J., Karpurapu, R., and Jarrett, P. M. (1992). ''Finite element analysis of a geogrid reinforced soil wall.'' *Grouting, Soil Improvement and Geosynthetics*, ASCE, 1213–1224.

Bolton, M., Choudhury, S., and Pang, P. (1978). ''Reinforced earth walls: A centrifugal model study.'' *Proc., Symposium on Earth Reinforcement*, ASCE, Pittsburgh, 252–281.

Christopher, B. R., Bonczkiewicz, C., and Holtz, R. (1994). ''Design, construction and monitoring of full scale test of reinforced soil walls and slopes.'' *Proc., of the Conf. on Recent Case Histories of Permanent Geosynthetic-Reinforced Soil Retaining Walls*, F. Tatsuoka and D. Leshchinsky, eds., A. A. Balkema, Rotterdam, The Netherlands, 45–60.

Christopher, B. R., and Leshchinsky, D. (1991). ''Design of geosynthetically reinforced slopes.'' *Proc., Geotechnological Engineering Congress 1991*, sponsored by the Geotechnological Engineering Division of the ASCE, Boulder, Colo, 988–1005.

Collin, J. G. (1997). *Design manual for segmental retaining walls*, National Concrete Masonry Association, 2nd ed., Herndon, Va.

Delmas, Ph., Gourc, J. P., Blivet, J. C., and Matichard, Y. (1988). ''Geotextile-reinforced retaining structures: A few instrumented examples.'' *Proc., Int. Geotechnological Symposium on Theory and Practice of Earth Reinforcement*, Fukuoka, Japan, 511–516.

Dove, J. E., and Frost, J. D. (1999). ''Peak friction behavior of smooth geomembrane-particle interfaces.'' *J. Geotech. Geoenviron. Eng.*, 125(7), 544–555.

Elias, V., Christopher, B. R., and Berg, R. R. (2001). ''Mechanically stabilized earth walls and reinforced soil slopes.'' *Publication Number Federal Highway Administration (FHWA) NH-00-043*, NHI-FHWA, Washington, DC.

Fannin, R. J., and Hermann, S. (1988). ''Field behavior of two instrumented, reinforced soil slopes.'' *Proc., of the Int. Geotech. Symposium on Theory and Practice of Earth Reinforcement*, Japan, 277–282.

Fannin, R. J., and Hermann, S. (1990). ''Performance data for a sloped reinforced soil wall.'' *Can. Geotech. J.*, (27), 676–686.

Fishman, K. L., Desai, C. S., and Sogge, R. L. (1993). ''Field behavior of instrumented geogrid soil reinforced wall.'' *J. Geotech. Eng.*, 119(8), 1293–1307.

Ghinelli, A., and Sacchetti, M. (1998). ''Finite element analysis of instrumented geogrid reinforced slope.'' *Proc., 6th Int. Conf. on Geosynthetics*, Atlanta, (2), 649–654.

Goodings, D. J., and Santamarina, J. C. (1989). ''Reinforced earth and adjacent soils: Centrifuge modeling study.'' *J. Geotech. Eng.*, 115(7), 1021–1025.

Güler, E., and Goodings, D. J. (1992). ''Centrifuge models of clay-lime reinforced soil walls.'' *Grouting, Soil Improvement and Geosynthetics*, R. H. Borden et al., eds., Geotechnological Special Publication No. 30, ASCE, New York, (2), 1249–1260.

Gustafsson, L., and Knutsson, S. (1994). ''An image analysis method for studying movement in granular and solid bodies.'' *Geotech. Test. J.*, 17(1), 95–100.

Jang, D. J., Frost, J. D., and Park, J. K. (1999). ''Preparation of epoxy impregnated sand coupons for image analysis.'' *Geotech. Test. J.*, 22(2), 147–158.

Jewell, R. A. (1991). ''Application of revised design charts for steep reinforced slopes.'' *Geotex. Geomembr.*, (10), 203–233.

Juran, I., and Christopher, B. R. (1989). ''Laboratory model study on

geosynthetic reinforced soil retaining walls.'' *J. Geotech. Eng.*, 115(7), 905–926.

Kasahara, K., Nomura, S., Kataoka, H., Arai, K., and Machihara, H. (1994). ''Field instrument for constructing the retaining wall reinforced with geotextiles.'' *Proc. of the Conf. on Recent Case Histories of Permanent Geosynthetic-Reinforced Soil Retaining Walls*, F. Tatsuoka and D. Leshchinsky, eds., 227–231.

Kemeny, J. M., Devgan, A., Hagaman, R. M., and Wu, X. (1993). ''Analysis of rock fragmentation using digital image processing.'' *J. Geotech. Eng.*, 119(7), 1144–1160.

Kuo, C.-Y., and Frost, J. D. (1996). ''Uniformity evaluation of cohesionless specimens using digital image analysis.'' *J. Geotech. Eng.*, 122(5), 390–396.

Kutter, B., Casey, J., and Romstad, K. (1990). ''Centrifuge modeling and field observations of dynamic behavior of reinforced soil and concrete cantilever retaining walls.'' *Proc., Fourth U.S. National Conf. on Earthquake Engineering*, Palm Springs, Calif. 663–672.

Law, H., Tohda, J., Ko, H.-Y., and Goddery, T. (1992). ''Prediction of the performance of a geosynthetic-reinforced wall by centrifuge experiments.'' *Proc., Int. Symposium on Geosynthetic-Reinforced Soil Retaining Walls*, J. T. H., Wu, ed., A. A. Balkema, Denver, 347–360.

Lee, K. L., Adams, B. D., and Vagneron, J. J. (1973). ''Reinforced earth retaining walls.'' *J. Soil Mech. Found. Div., Am. Soc. Civ. Eng.* 99(SM10), 745–764.

Leshchinsky, D., and Boedeker, R. H. (1989). ''Geosynthetic reinforced soil structures.'' *J. Geotech. Eng.*, 115(10), 1459–1478.

Liang, L., Saada, A., Figueroa, J. L., and Cope, C. T. (1997). ''The use of digital image processing in monitoring shear band development.'' *Geotech. Test. J.*, 20(3), 324–339.

Mahmud, M. B., and Zimmie, T. F. (1998). ''Instrumentation and calibration of geotextiles used in centrifuge modeling of slopes.'' *Transportation Research Record 1614*, Transportation Research Board, Washington, D.C., 3–7.

Miki, H., Kutara, K., Minimi, T., Nishimura, J., and Fukuda, N. (1988). ''Experimental studies on the performance of polymer grid reinforced embankment.'' *Proc., Int. Symposium on Theory and Practice of Earth Reinforcement*, Fukuoka, Japan, 431–436.

Mitchell, J. K., Jaber, M., Shen, C. K., and Hua, Z. K. (1988). ''Behavior of reinforced soil walls in centrifuge model tests.'' *Proc., Centrifuge 88*, J. F., Corte, ed., A. A. Balkema, Paris, 259–271.

Mora, C. F., Kwan, A. K. H., and Chan, H. C. (1998). ''Particle size distribution analysis of coarse aggregate using digital image processing.'' *Cem. Concr. Res.*, 28(6), 921–932.

Nova-Roessig, L., and Sitar, N. (1998). ''Centrifuge studies of the seismic response of reinforced soil slopes.'' *ASCE Geotechnichal Special Publication No. 75*, Geotechnological Earthquake Engineering and Soil Dynamics III, P. Dakuolas, M. Yegian, and R. Holtz, eds., Seattle, (1), 458–468.

Obaidat, M. T., Al-Masaeid, H. R., Gharaybeh, F., and Khedaywi, T. S. (1998). ''An innovative digital image analysis approach to quantify the percentage of voids in mineral aggregates of bituminous mixtures.'' *Can. J. Civ. Eng.*, (25), 1041–1049.

Porbaha, A., and Goodings, D. J. (1996). ''Centrifuge modeling of geotextile-reinforced cohesive soil retaining walls.'' *J. Geotech. Eng.*, 122(10), 840–848.

Ragheb, A., and Elgamal, A. (1991). ''Effects of gradual reinforcement compromise on the behavior of mechanically stabilized earth walls.'' *Proc., Centrifuge 91*, H.-Y., Ko, and F. G., McLean, eds., Boulder, Colo., A.A. Balkema, Rotterdam, The Netherlands, 333–340.

Raschke, S. A., Hryciw, R. D., and Donohoe, G. W. (1996). ''Microdeformations in sands by digital image processing and analysis.'' *Transportation Research Record*, Transportation Research Board, Washington, D.C., 1548, 31–37.

Schmertmann, G. R., Chouery-Curtis, V. E., Johnson, R. D., and Bonaparte, R. (1987). ''Design charts for geogrid-reinforced soil slopes.'' *Proc., Geosynthetics'87 Conf.*, JFAI, New Orleans, 108–120.

Thomas, T. W., White, T. D., and Kuczek, T. (1994). ''Siliceous content determination of sands using automatic image analysis.'' *Transportation Research Record 1437*, Transportation Research Board, Washington, D.C., 51–58.

Wright, S. G., and Duncan, J. M. (1991). ''Limit equilibrium stability analyses for reinforced slopes.'' *Transportation Research Record 1330*, Transportation Research Board, Washington, D.C., 40–46.

Zornberg, J. G., Barrows, R. J., Christopher, B. R., and Wayne, M. H. (1995). ''Construction and instrumentation of a highway slope reinforced with high-strength geotextile.'' *Proc. of the Int. Conf. Geosynthetics'95*, Nashville, Tenn., 13–27.

Zornberg, J. G., and Kavazanjian, E. (2001). ''Prediction of the performance of a geogrid-reinforced slope founded on solid waste.'' *Soils Found.*, 41(6), 1–16.

Zornberg, J. G., and Mitchell, J. K. (1994). ''Finite element prediction of the performance of an instrumented geotextile-reinforced wall.'' *Proc., 8th Int. Conf. of the Int. Association for Computer Methods and Advances in Geomechanics (IACMAG '94)*, Morgantown, W. Va., A.A. Balkema, Rotterdam, The Netherlands, 2, 1433–1438.

Zornberg, J. G., Mitchell, J. K., and Sitar, N. (1997). ''Testing of reinforced slopes in a geotechnical centrifuge.'' *Geotech. Test. J.*, 20(4), 470–480.

Zornberg, J. G., Sitar, N., and Mitchell, J. K. (1998a). ''Performance of geosynthetic reinforced slopes at failure.'' *J. Geotech. Geoenviron. Eng.*, 124(8), 670–683.

Zornberg, J. G., Sitar, N., and Mitchell, J. K. (1998b). ''Limit equilibrium as basis for design of geosynthetic-reinforced slopes.'' *J. Geotech. Geoenviron. Eng.*, 124(8), 684–698.